Hindrance function for sedimentation and creaming of colloidal disks

Peng He, Andres F. Mejia, and Zhengdong Cheng*
Artie McFerrin Department of Chemical Engineering, Texas A&M University, College Station, Texas 77843, USA

Dazhi Sun and Hung-Jue Sue
Department of Mechanical Engineering, Texas A&M University, College Station, Texas 77843, USA

Dean S. Dinair
LUM Corporation, 2525 Arapahoe Avenue, Unit E4, Boulder, Colorado 80302, USA

Manuel Marquez
YNano LLC, 14148 Riverdowns South Dr., Midlothian, Virginia 23113-3796, USA
(Received 25 July 2009; published 19 February 2010)

We report the first measurement of the hindrance function for sedimentation or creaming of disk-shaped colloids via the analytical centrifugation. Disks align with the external flow right above a volume fraction of a few percent, and this effect is extremely sensitive to the aspect ratio of disks. Due to this alignment effect, disk sedimentation or creaming demonstrates distinct trends in dilute and semidilute regions.

DOI: 10.1103/PhysRevE.81.026310 PACS number(s): 47.57.ef, 82.70.Dd, 82.70.Kj, 83.80.Hj

Sedimentation of colloidal particles involves in many natural and industry processes, such as in medical diagnostics [1], macromolecule morphology analysis [2], mineral processing, and environmental monitoring [3]. Understanding of sedimentation dynamics provides useful information for different physical phenomena in the suspensions such as phase separations [4], long-range velocity correlations [5], and epitaxial growth of colloidal crystals [6]. Sedimentation of spherical particles has been investigated for more than a century [7,8], yet the sedimentation of anisotropic particles is less thoroughly studied although anisotropic particles play important roles in many complex fluids [9]. Sedimentation of rodlike colloids is under the most investigations among anisotropic particles, in such topics as the sedimentation equilibrium of uniform tobacco mosaic virus [10] and sedimentation in mixture with polymers [11]. Anisotropic particle sedimentations demonstrated distinct characteristics due to the hydrodynamic interactions and long-range correlations, such as the formation of microstructure and streamer in settling rods and fibers at high Péclet number [12–14], as well as the dependence on aspect ratio and orientation [15,16]. Among the anisotropic particles, discotic colloids aroused significantly interests due to the study of human red blood cells aggregation, clay platelets in soil and minerals [17], asphaltene in petroleum production and refinery [18], and calcium oxalate crystals in the kidney stone [19]. Rheological properties of clay suspensions were intensively studied and important information about the hydrodynamic interactions and volume fraction dependence under shear flow was obtained [20]. Although this information is helpful, the knowledge and understanding of disklike particle sedimentation behavior is still far from complete, comparing to spherical and rodlike particle systems.

One of the most important sedimentation characteristics is the hindrance function, which describes the dependence of settling or creaming speed on concentrations. For spheres with hard-core interactions, Batchelor obtained the analytical result of first-order dependence on volume fraction ϕ, $U/U_0=1-K\phi+O(\phi^2)$ with $K=6.55$, assuming a random distribution of particles and two-body hydrodynamic interactions [21]. Here the settling or creaming speed is normalized by Stokes velocity $U_0=\Delta\rho g D^2/18\mu$, in which D is the diameter of the sphere, $\Delta\rho$ is the density difference between the sphere and the solvent, g is the gravity constant, and μ is the solvent viscosity. This first-order dependence has been confirmed by experiments on hard spheres [4,22]. Richardson and Zaki correlated the sphere settling speed and ϕ in fluidized beds and particle suspensions [23] by $U/U_0=(1-\phi)^n$, where the empirical parameter n is around 4.65, and later Buscall *et al.* modified n to 5.5 for wide ranges of volume fractions [24]. Batchelor and Wen obtained $U/U_0\approx 1-5.6\phi$ for dilute polydisperse spherical suspensions, where the density variance is negligible in respect to the size variance [25].

For discotic colloidal particles, such dependence has not been systematically obtained either experimentally or theoretically. Capuani *et al.* simulated charged discotic colloids using the lattice-Boltzmann method [26]. Van der Kooij *et al.* investigated the phase transition in platelike gibbsite colloidal suspensions with polydispersity up to 25%, which showed an isotropic-nematic (I-N) transition around $\phi\approx 20\%$ [27]. The index K in analogy to Batchelor's formula was found to be greater for settling disks than that for rigid spheres using dilute gibbsite platelets suspensions of $\phi\leq 5\%$, indicating a stronger backflow in disk sedimentation [27,28]. So far, there are no data for discotic colloids sedimentation at high concentrations, $\phi>5\%$. In this paper, we present experimental results of disk sedimentation or creaming in dilute and semidilute systems up to $\phi\approx 20\%$. The sedimentation or creaming speed was measured using analytical centrifugation (Fig. 1) [29,30]. A hindrance function is

*Author to whom correspondence should be addressed; cheng@chemail.tamu.edu

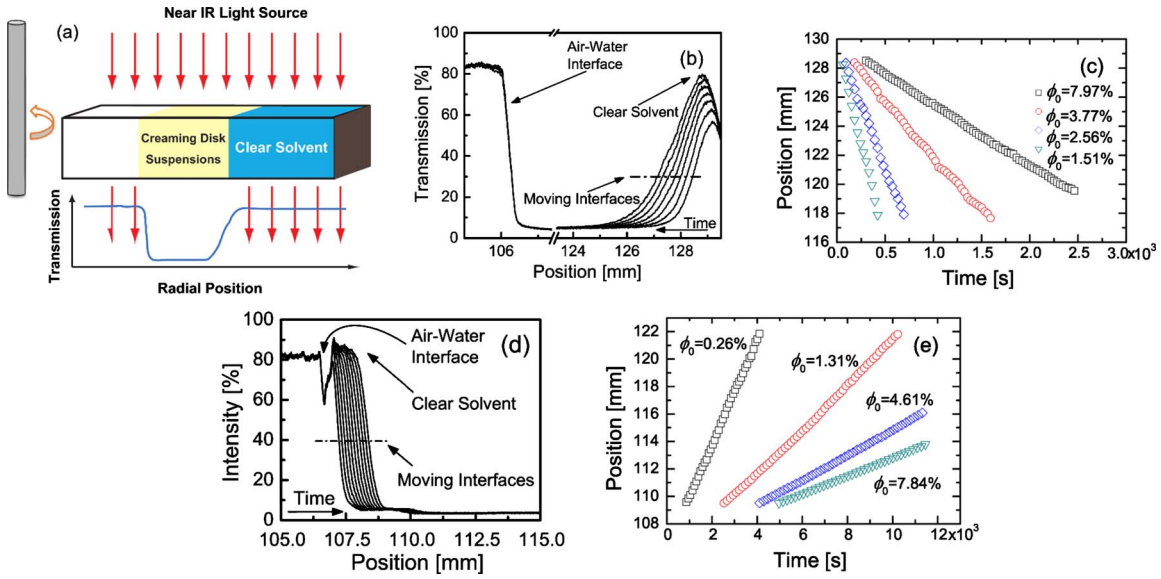

FIG. 1. (Color online) Sedimentation or creaming of colloidal disks in an analytical centrifuge. (a) Instrument scheme. (b) Sequential transmission profiles in the measurement of creaming of a wax sample [~8% (v/v)], where the dash-dotted line in the center represents the transmission intensity for tracking the position of solvent-suspension interface. (c) Measured radial positions of the solvent-suspension interface in wax samples as a function of time. The slopes yield the creaming speeds. The initial volume fractions ϕ_0 are labeled. (d) Sequential transmission profiles in the measurement of sedimentation in ZrP samples [~1.3% (v/v)], where the dash-dotted line in the center represents the transmission intensity for tracking the position of solvent-suspension interface. (e) Measured radial positions of the solvent-suspension interface in ZrP samples as a function of time. The slopes yield the sedimentation speeds. The initial volume fractions ϕ_0 are labeled.

obtained in the consideration of both backflow effect and disk orientation in suspensions.

The colloidal disk-shaped particles used in our experiments are α-eicosene (wax) particles and α-zirconium phosphate (ZrP) nanoplatelets [31–34], whose morphological properties are listed in Table I. For disks with thickness t and diameter D, the aspect ratio is defined as $\xi = D/t$. The ZrP nanoplatelets were synthesized by hydrothermal reactions [32,33] and utilized for data of higher aspect ratio disks ($\xi > 5$). The extremely high aspect ratio disks were prepared by exfoliating ZrP into monolayer platelets in an aqueous solution, using tetra-*n*-butylammonium hydroxide (TBA) of proper stoichiometric ratio such that the entire ZrP surface was covered by a monolayer of TBA molecules [33]. The wax disks were made by ultrasound emulsification followed by shape transition at 4 °C, and various concentrations of sodium dodecyl sulfate (SDS) surfactant were used to adjust the wax disk aspect ratio during the shape transition [34]. Before the analytical centrifugation measurements, wax disk suspensions were first concentrated to about 20% (v/v), then diluted to a series of volume fractions. The ZrP powder was used at different weight percentages converted to volume fractions using $\rho_{ZrP} = 2.55$ g/cm^3. The suspensions were finally suspended in 1 mM NaCl salt solutions via solvent exchange to screen the charges on the particle surfaces, and the resulting Debye screening length was estimated to be 9.7 ± 0.26 nm. Hence, the inter-particle interaction is assumed to be hard-core repulsion.

TABLE I. Morphological properties of disk samples used in the experiments.

Sample	Diameter D (nm)	Thickness t (nm)	Aspect ratio[a] ξ
Wax[b] A	198.4 ± 47.8	72.67 ± 19.83	2.73 ± 0.35
Wax B	152.9 ± 28.9	32.12 ± 7.15	4.76 ± 0.56
ZrP[c], nonexfoliated	350 ± 98	36 ± 5.5	9.0 ± 1.1
ZrP, exfoliated	350 ± 98	2.68 ± 0.24	130.6 ± 35.6

[a]The aspect ratio of disk particles, ξ, is defined as the ratio between the diameter D and the thickness t.
[b]The diameters of wax disks were measured by DLS. Aspect ratios of wax disks were measured using their shape transition (see Appendix).
[c]The aspect ratio of ZrP was determined by TEM (for the thickness) and DLS (for the diameter).

Sedimentation or creaming speeds were measured by the analytical centrifugation analyzer LUMiSizer® (LUM Corporation, CO). Similar instrumentations have been utilized in the characterization of gibbsite platelets [27,28]. The apparatus consists of a cell chamber, a centrifugal rotor, a pulsed near-infrared light-emitting diode (880 nm) as light source, and a charge-coupled device line (CCD-Line) as the light collector. Suspensions were pipetted into polycarbonate measurement vials, and the sample volume was adjusted to $10 \times 25 \times 2$ mm^3 in width × length × height. All samples were well mixed right before the sedimentation or creaming measurement. The temperature of the measurements was all set at $T = 22 \pm 0.4$ °C except for the spherical wax emulsions, which were measured at $T = 30 \pm 0.4$ °C, above the melting temperature of α-eicosene, $T_m = 26$ °C. The sequential space and time transmission profiles of wax or ZrP disk suspensions in a single measurement at a typical rotation speed of

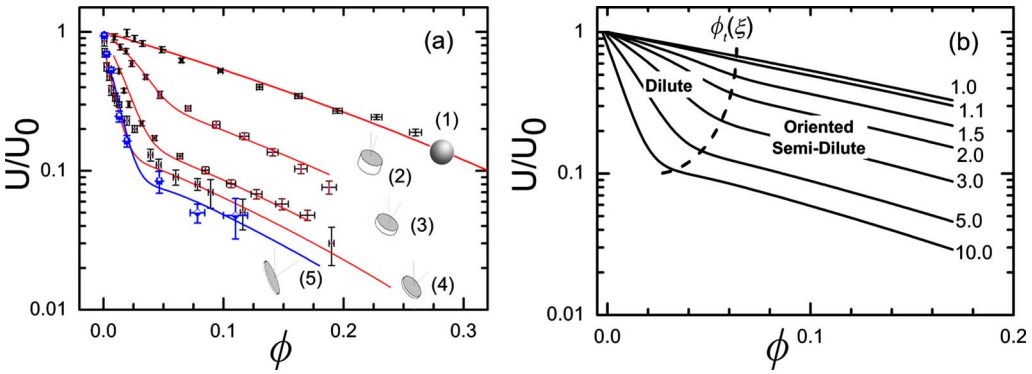

FIG. 2. (Color online) The dimensionless sedimentation or creaming speed as a function of particle volume fraction for suspensions of spherical wax droplets (ξ=1 for curve 1), ZrP platelets ($\xi \approx 9$ for curve 4 and $\xi \approx 130$ for curve 5), and wax disks ($\xi \approx 2.73$ for curve 2 and $\xi \approx 4.76$ for curve 3). (a) Experimental data. The disk orientations are illustrated according to the results in Fig. 3(b) (lower inset). (b) Hindrance function curves of Eq. (1) exhibits the influence of anisotropy. The numbers to the right of each solid curve represent the aspect ratios. A semidilute region and the dilute region are separated by the dashed line of $\phi_t(\xi)$.

4000 rpm are shown in Fig. 1(b) or Fig. 1(d). The migration of particles led to the formation of an opaque sedimenting or creaming layer (low transmission) and a clear liquid layer (high transmission). Transmission profile measurements were obtained instantaneously across the sample with a spatial resolution ≤ 10 μm. The transmission profiles at the beginning of the time elapse (within 20 min from the starting time) were chosen for the analysis so that they presented the initial volume fraction in the uniform mixture before the significant increase in volume fraction and the emerge of large-scale microstructure. The positions of the suspension-solvent interface were tracked at a specific transmission value determined by the geometric mean of the highest and lowest values of transmission, which is marked by the horizontal dash-dotted line in Fig. 1(b) or Fig. 1(d). The sedimenting and creaming speed was calculated from the slope of the position vs time plot using the specialized data analysis software provided by LUM Corporation [35], as shown in Fig. 1(c) or Fig. 1(e). An apparent slight spreading of the interfaces in Fig. 1(b) or Fig. 1(d) was due to the relatively large polydispersity in our sample ($\sim$30% for ZrP and $\sim$25% for wax, measured by dynamic light scattering (DLS), and the analysis of this polydispersity effect revealed that it could increase the number averaged coefficient of sedimentation by a factor of $(1+2\sigma^2)$, where σ is the polydispersity of the samples, thus an increase of about 18% for ZrP and 12% for wax [28].

The measured dimensionless sedimentation or creaming speed U/U_0 is plotted in Fig. 2(a). The terminal sedimentation or creaming speed of a single disk is calculated in approximation of an oblate ellipsoid with the same thickness and diameter [36] (see Appendix). Data for spherical droplets are also shown for comparison. Error bars of the speeds are based on the linear fitting error of the solvent-suspension interface position tracking [Figs. 1(c) and 1(e)]. The error in volume fractions is calculated from sample preparation procedures. All measurements show that the normalized disk sedimentation or creaming speed is remarkably slower than that of spheres at the same volume fraction. In particular, we observe two distinct sedimentation and creaming trends for dilute and semidilute disk suspensions (Fig. 2).

At low volume fractions, U/U_0 displays a dramatic drop with increasing ϕ. For batch sedimentation or creaming, a solvent flux, which is called backflow, flows opposite to the sedimentation or creaming direction to compensate the volume flux of settling or creaming colloidal particles. The hydrodynamic interaction between backflow and the moving particles will exert a force on the particles to retard their sedimentation or creaming speed, resulting in the drop of U/U_0 with increasing ϕ. A set of sphere data is given as reference [Fig. 2(a), curve 1], which is directly measured using the spherical droplets in our wax emulsions (made by melting wax suspensions at 30 °C) whose polydispersity is $13.73 \pm 3.03\%$, determined by DLS. The ratio U/U_0 in the sphere data is scaled as $(1-\phi)^{K_{\text{sphere}}}$ to find the index $K_{\text{sphere}}=5.95 \pm 0.27$, slightly below the theoretical value 6.5 of monodisperse spheres. For disks, the U/U_0 curves could still be scaled by the power law of $(1-\phi)$ in the dilute regime with much larger exponents than that of spheres, suggesting a stronger backflow for disks sedimentation or creaming since the disks could occupy additional exclude volume comparing with spheres [28]. Our experiments also show that such slopes increase with increasing disk aspect ratio [Fig. 3(a)], implying that disk shape can significantly alter their backflow. The slopes increase toward a limit value at large aspect ratio, as shown in Fig. 2(a), where the slope of ξ=9 is very close to that of ξ=130.

At higher volume fractions, the dramatic drop in U/U_0 with increasing ϕ abates in contrast to the dilute regime. All disk sedimentation and creaming curves are approximately parallel to one another, and their slopes are closer to that of the sphere speed data. This is the first experimental observation that a weaker retardation of sedimentation or creaming speed occurs in disk suspensions at high volume fractions. We hypothesize that this reduction originates from the restricted orientation of the disks at high volume fractions, in agreement with the evidences in previous experimental observations of disk shear flow and sedimentation [20,37]. Such restricted orientation could reduce the additional exclude volume of the disk particles and alter the effect of backflow. The aspect ratio dependence in the high volume fraction regime has the same trend as in the dilute regime, i.e., the larger the aspect ratio, the smaller the normalized

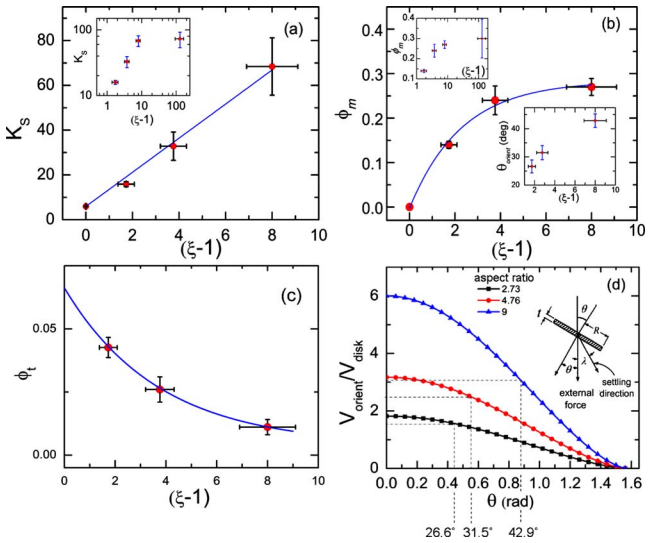

FIG. 3. (Color online) The dependence of hindrance function on the aspect ratio ξ of disks. (a) K_S describes the backflow effect at dilute concentrations of disks as does in Eq. (2). (Inset) The limiting value of K_S with very high aspect ratio $\xi \sim 130$. (b) ϕ_m denotes the extra exclude volume for oriented disks compared to spheres. (Inset up) The limiting value of ϕ_m with very high aspect ratio $\xi \sim 130$. (Inset down) Disk orientation angle converted from the correlation of Eq. (11) between ϕ_m and $(V_{\text{orient}}/V_{\text{disk}})$. (c) ϕ_t, the transition volume fraction above which disks orient. (d) Dependence of $(V_{\text{orient}}/V_{\text{disk}})$ on the disk orientation angle θ. (Inset) Scheme of oblique falling of a disk.

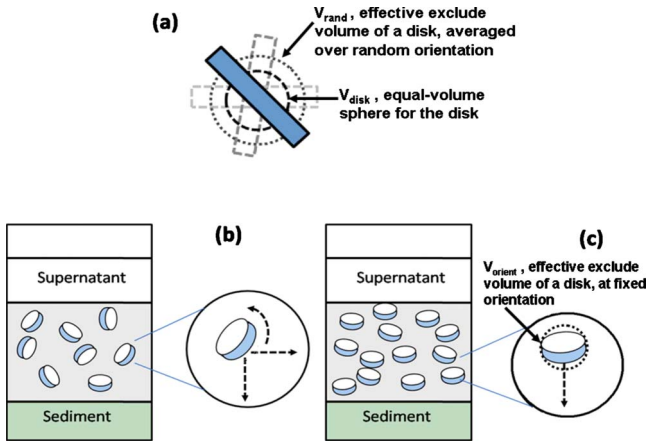

FIG. 4. (Color online) Orientation and motions of settling or creaming disk-shaped particles. (a) Representation of different "volumes" related to settling/creaming disks. (b) At low volume fractions, the disk-shaped particles are randomly oriented. The effective exclude volume, V_{rand}, is larger than the disk volume, V_{disk}. Hence, a higher resistance to the sedimentation or creaming speed is resulted from a stronger backflow comparing to the equal-volume spherical suspensions. (c) At high volume fractions, the disk-shaped particles tend to orient under the external force. Since $V_{\text{disk}} < V_{\text{orient}} < V_{\text{rand}}$, sedimentation or creaming speed deviates from dilute suspensions but closes to the behavior of spheres.

sedimentation or creaming speed. The differences between curves of various aspect ratios diminish at high aspect ratios. The curves move toward a limiting curve as the aspect ratio becomes very large [Fig. 2(a)].

Considering both trends in low and high volume fraction regimes, the following hindrance function for disk sedimentation and creaming is obtained;

$$\frac{U}{U_0} = (1-W)(1-\phi)^{K_S} + W[1-(\phi+\phi_m)]^{K_{\text{sphere}}}, \qquad (1)$$

$$\text{in which } W = \left[1+\exp\left(-\frac{\phi-\phi_t}{\kappa}\right)\right]^{-1}.$$

In Eq. (1), the first term on right side is chosen to be consistent with the hindrance function of spherical particles through the parameter K_S for dilute regime, and the second term on right side takes a similar form but emphasizes the effect of restricted orientation on the exclude volume through the parameter ϕ_m for the semidilute regime. Function W in Eq. (1) is similar to a logistic function to describe the transition between dilute and semidilute regime above which the restricted orientation of disk particles emerges. The position of the transition is controlled by ϕ_t and the sharpness of the transition is controlled by κ (an empirical value $\kappa \sim 0.008$ is chosen). We used $K_{\text{sphere}} = 5.95 \pm 0.27$ [Fig. 2(a), curve 1] from the measurement of our wax emulsions as mentioned above. The other parameters, K_S, ϕ_m, and ϕ_t are obtained from fitting Eq. (1) with experimental data and reveal the dependence of the hindrance function on the aspect ratio ξ. The values of the fitting parameters do not change significantly when $\xi > 10$, as shown in the insets of Figs. 3(a) and 3(b).

At low volume fractions, the disk-shaped particles are randomly oriented due to the Brownian motion. Hence, compared to spheres, disks will occupy a larger projection area than the equal-volume spheres in the plane perpendicular to the external force, thus interact more strongly with the solvent [20,28]. The effective spherical volume V_{rand} for such sedimentation or creaming disk must include both the volume of the disk itself, V_{disk}, and the additional exclude volume consisting of bound fluid carried with the particles [Fig. 4(b)]. The larger exclude volume V_{rand} will require more compensation flux for balance, thus a larger backflow will be induced and the disk sedimentation or creaming is expected to be dramatically slower than that of rigid spherical particle suspensions.

The theoretical calculation of the backflow effect has not been performed for disk particles so far. Here, we attempt to estimate it using the effective spherical volume V_{rand} and a pair-correlation function $g_{\text{rand}}(z_{\text{eq}})$. In our experiments, the Reynolds number $\text{Re} = \frac{\rho U D}{\mu}$ is very small, around 10^{-7}, and the Péclet number $\text{Pe} = \Delta m g D / k_B T$ is moderate, around 1–10. For sphere sedimentation at small Reynolds number, the index K_S can be derived from the creeping flow and the Oseen equations as [38]

$$K_S = \frac{1}{2} - 3\int_{z\geq 1} z[g(z)-1]dz - \int_0^\infty z^2 g(z)[A(z)+2B(z) + C(z)]dz. \qquad (2)$$

Equation (2) considers only two-body hydrodynamic interac-

tions. The last term in Eq. (2) accounts for the hydrodynamic reflection of its own backflow from all surrounding neighbor particles. $z=l/r$ is the ratio of the center-to-center distance l between a pair of spheres and the sphere radius r, $A(z)$, $B(z)$, $C(z)$ are the hydrodynamic mobility functions given by

$$A(z) = -\frac{15}{4}z^{-4} + \frac{11}{2}z^{-6} + O(z^{-8}), \tag{3}$$

$$B(z) = -\frac{17}{16}z^{-6} + O(z^{-8}), \tag{4}$$

$$C(z) = \frac{75}{4}z^{-6} + O(z^{-9}), \tag{5}$$

and $g(z)$ is the pair-correlation function of the hard sphere potential,

$$g(z) = \begin{cases} 0, & z < 2 \\ 1, & z \geq 2. \end{cases} \tag{6}$$

Since $V_{\text{rand}} > V_{\text{disk}}$, the exclude distance of the effective spherical volume, $2r_{\text{rand}}$, will be larger than that of the equal-volume sphere suspensions, $2r_{\text{eq}}$, but smaller than the radius of the disk, R. Previous study on the averaged effect of the random oriented platelike particles [37] revealed $r_{\text{rand}}/R = \sqrt{5/6} \sim 0.913$. From the equal-volume relationship, $\frac{4}{3}\pi r_{\text{eq}}^3 = \pi R^2 t = 2\pi R^3/\xi$, we have $R/r_{\text{eq}} \sim O(\xi^{1/3})$ and $\lambda = r_{\text{rand}}/r_{\text{eq}} \sim 0.913\xi^{1/3}$. Substituting $z=l/r_{\text{rand}}$ with $z_{\text{eq}}=l/r_{\text{eq}}=\lambda z$ in Eq. (6), the pair-correlation function is modified as g_{rand} to describe disks,

$$g_{\text{rand}}(z_{\text{eq}}) = \begin{cases} 0, & z_{\text{eq}} < 2\lambda \\ 1, & z_{\text{eq}} \geq 2\lambda. \end{cases} \tag{7}$$

Since the volume fraction ϕ in the hindrance function is based on V_{disk}, the substitution of V_{disk} by V_{rand} will introduce a factor of $\lambda^3 = (r_{\text{rand}}/r_{\text{eq}})^3$ in the calculation of $K_S(\xi)$. With the substitution of Eq. (6) by Eq. (7) and z by z_{eq}/λ, we obtain

$$\begin{aligned} K_S(\xi) = \lambda^3 \Bigg\{ & \frac{1}{2} - 3\int_{z_{\text{eq}} \geq \lambda} \frac{z_{\text{eq}}}{\lambda^2}[g_{\text{rand}}(z_{\text{eq}}) - 1]dz_{\text{eq}} \\ & - \int_0^{\infty} \frac{z_{\text{eq}}^2}{\lambda^3} g_{\text{rand}}(z_{\text{eq}})[A(z_{\text{eq}}/\lambda) + 2B(z_{\text{eq}}/\lambda) \\ & + C(z_{\text{eq}}/\lambda)]dz_{\text{eq}} \Bigg\}. \end{aligned} \tag{8}$$

We expect an amplification of K_{sphere} to K_S due to the larger exclude volume for the disk sedimentation or creaming. Our experiments indeed indicate a linear dependence of K_S on ξ for $\xi < 10$, $K_S = (5.95 \pm 0.27) + (7.614 \pm 0.255)(\xi - 1)$, which can be roughly predicted by the first two terms in Eq. (8) since the third term is much smaller comparing to them,

$$\begin{aligned} K_S &\approx 0.38\xi - 3\int_{z_{\text{eq}} \geq \lambda} (\lambda z_{\text{eq}})[g_{\text{rand}}(z_{\text{eq}}) - 1]dz_{\text{eq}} \\ &= 0.38\xi + 3\lambda \int_{\lambda}^{2\lambda} z_{\text{eq}} dz_{\text{eq}} = 4.88\xi \sim O(\xi). \end{aligned} \tag{9}$$

Several aspects might contribute to the discrepancy, including polydispersity of the sample (increasing K_S by 10–20 % [28]), different pair correlations accounting for the anisotropy of disks [39], or the hydrodynamic mobility functions to be more suitable for discotic colloids [40].

Different from the dilute regime, previous experiments revealed that disk-shaped particles tend to align themselves with external flow at high volume fractions [20,40] and have a restricted orientation. In Eq. (1), the parameter ϕ_m accounts for the extra exclude volume for the oriented disks comparing to the equal-volume spheres, and our experiment indicates its dependence on ξ for $\xi < 10$, $\phi_m = (0.284 \pm 0.021)[1 - \exp(\frac{1-\xi}{2.29 \pm 0.487})]$. With a similar meaning to V_{rand}, we define the projection volume of oriented disks perpendicular to the external force as V_{orient}. For a rigid sphere and an oriented disk with equal volume, the ratio between their cross section areas in the plane perpendicular to the external force varies with this orientation angle θ,

$$\frac{4}{3}\pi r^3 = \pi R^2 t = \frac{2\pi R^3}{\xi} \Rightarrow r = \sqrt[3]{\frac{3R^2 t}{4}}, \tag{10}$$

$$\frac{A_{\text{orient}}}{A_{\text{disk}}} = \frac{\pi R^2 \cos\theta}{\pi R \sqrt[3]{\frac{9}{16}Rt^2}} \approx 0.763\xi^{2/3}\cos\theta, \quad \theta \in [0, \pi/2]. \tag{11}$$

Converting this ratio from cross section area to exclude volumes by assuming spherical shapes, we obtain $(V_{\text{orient}}/V_{\text{disk}}) \sim (A_{\text{orient}}/A_{\text{disk}})^{3/2} \sim 0.67\xi(\cos\theta)^{3/2}$. The oriented disk has a smaller effective exclude volume than random-oriented disks, i.e., $V_{\text{disk}} < V_{\text{orient}} < V_{\text{rand}}$, hence the compensation flux of backflow is smaller and the U/U_0 normalization is higher compared to random oriented disks, which is reflected as the weaker retardation of sedimentation or creaming speed occurring in disk suspensions at high volume fractions [Fig. 2(a)]. Plotting $V_{\text{orient}}/V_{\text{disk}}$ in Fig. 3(d), we can see that as the aspect ratio of the disks increases, the change in this volume ratio becomes more remarkable with orientation angle. The volume fraction range of oriented disk sedimentation or creaming is approximately [0.05,0.3], with a normalized speed U/U_0 corresponding to the sphere sedimentation or creaming in a volume fraction range [0.3,0.5] [Fig. 2(a)]. Selecting the middle point in this range as a typical value, we obtain a *correlation*, $V_{\text{orient}}/V_{\text{disk}} \sim 0.4/(0.4 - \phi_m)$, which compares the gained exclude volume in the oriented disks, V_{orient}, with the equal-volume spheres, V_{disk}. The orientation angles θ_{orient} can then be estimated from the $V_{\text{orient}}/V_{\text{disk}}$ function [Fig. 3(d)] and are plotted in the inset of Fig. 3(b). We observe that the orientation angles θ_{orient} increase with the disk aspect ratio. This suggests that the small aspect ratio disks tend to settle or cream

with their surfaces more or less perpendicular to the migration direction, while the disks with larger aspect ratio will be more willing to orient themselves with the surrounding flow field. Our normalized settling/creaming speed plot also shows that, for particles with the same aspect ratio, above the dilute to semidilute transition the slope of the U/U_0 curve does not change with increasing volume fractions, which indicates that the alignment and the orientation angle do not depend on volume fractions, similar to the results in clay suspension shearing experiments [20].

In our hindrance function [Eq. (1)], the trends in the dilute regime and semidilute regimes are connected at the transition point ϕ_t. All curves show a dramatic retardation in the dilute regime for random oriented disks and a moderate reduction in the semidilute regime for oriented disks. ϕ_t depends on the disk aspect ratio ξ for $\xi<10$ as $\phi_t(\xi)=0.062-0.0123(\xi-1)+7.4571\times10^{-4}(\xi-1)^2$. It becomes smaller as the disk aspect ratio increases, which means the disks of higher aspect ratio are more willing to possess an orientation in settling or creaming compared to the disks having a smaller aspect ratio. Therefore, the orientation effect will manifest itself at lower volume fractions for high aspect ratio disks. This dependence on aspect ratio is also consistent with the prediction of clay suspensions under shearing flow [20], which explained that the transition volume fraction is an inverse function of the aspect ratio of particle when the Debye length is much smaller than the dimension of the particle:

$$\phi^* = 0.64\left(\frac{3}{2}\right)\left(\frac{t}{D}\right)\left[\frac{1}{(1+2/D\delta)^3}\right], \tag{12}$$

where ϕ^* is the critical volume fraction for volume exclude interactions to occur, t and D are, respectively, the thickness and the diameter of particle, and δ^{-1} is the Debye length.

At low aspect ratios, the disks align nearly perpendicular to the external field, in contrast to a large tilt angle at high aspect ratio [lower inset in Fig. 3(b)]. Hence, a small deviation in aspect ratio from that of a rigid sphere ($\xi=1$) will greatly change the magnitude of the sedimentation or creaming speed curve (e.g., the curves for $\xi=1.5$ and $\xi=2$). It is important to further investigate this region in order to reveal the onset of the anisotropic effect for disks and oblate spheroids. There, the stability and hydrodynamic interactions will be significantly altered. Due to the difficulties of synthesizing such kind of disks in our experiments, it is hard to assess the deviation at small aspect ratio with $\xi<2$, but numerical simulations might reveal more interesting aspects and behaviors in this region.

In summary, we propose a general hindrance function to describe sedimentation and creaming over the whole volume fraction regime of discotic fluid phase. This hindrance function includes the strong backflow in dilute suspensions due to the random orientation under Brownian motion and the reduction in backflow effect at high volume fractions due to the restricted orientation. Our experiments indicate that the aspect ratio of discotic colloids plays an important role in their sedimentation and creaming behavior. The effective exclude volume, the restricted orientation, and the transition between dilute and semidilute regime are all sensitive to their aspect ratios for disk suspensions. Especially, the disks will behave quite differently with only a small deviation from the spherical shape. As a systematic investigation, this hindrance function will serve as a guide to better understand the stability and dynamics of discotic complex fluids commonly found in nature and industry.

Acknowledgment is made to the donors of the American Chemical Society ACS Petroleum Research Fund (PRF Grant No. 45303-G7) and by the Dow Chemical Co.. This work was also supported by start-up funds from Texas Engineering Experimental Station and Texas A&M University. We acknowledge the generous support from Dr. D. Lerche and LUM Corporation.

APPENDIX

The aspect ratio of wax disks, ξ=diameter/thickness, was determined by comparing its diffusion coefficient to that of the equal volume spheres. The diffusion coefficient D^*_{disk} of wax disks was first measured, then the wax disks were heated to become spherical droplets and the diffusion coefficient D_{sphere} was measured. The radius for spheres can be calculated using

$$r = \frac{k_B T}{6\pi\mu D_{\text{sphere}}}, \tag{A1}$$

where T is the temperature, k_B is the Boltzmann constant, and μ is the solvent viscosity. For a cylindrical disk with thickness t and diameter $2R$, $\xi=\frac{2R}{t}$, and D^*_{disk} is approximated by the formula of oblate ellipsoids with the same aspect ratio and thickness [41],

$$t = \frac{k_B T}{3\pi\mu D^*_{\text{disk}}}\frac{\arctan(\sqrt{\xi^2-1})}{\sqrt{\xi^2-1}}. \tag{A2}$$

Since the density difference between the wax solid and liquid is negligible [42], we can assume that the volume does not change during the shape transition from a cylindrical disk to a sphere, i.e.,

$$\frac{4}{3}\pi r^3 = \pi R^2 t = \frac{2\pi R^3}{\xi}. \tag{A3}$$

Combining Eq. (A1)–(A3), we obtain the equation for determining the wax disk aspect ratio ξ,

$$\frac{\arctan(\sqrt{\xi^2-1})}{\sqrt{\xi^2-1}}\xi^{2/3} = \left(\frac{2}{3}\right)^{1/3}\left(\frac{D^*_{\text{disk}}}{D_{\text{sphere}}}\right). \tag{A4}$$

The approximation of an oblate ellipsoid is adopted to calculate U_0, the terminal sedimentation or creaming speed of a single disk. For a disk with thickness $2b$ and diameter $2a$, the anisotropic translational friction coefficients are given by [36]

$$f_\perp = 16\pi\mu\frac{b^2-a^2}{(2b^2-a^2)S-2b} \tag{A5}$$

and

$$f_{\parallel} = 32\pi\mu \frac{b^2 - a^2}{(2b^2 - 3a^2)S + 2b}, \tag{A6}$$

where subscripts $\parallel$ and $\perp$ denote the directions parallel and perpendicular to the flat surface of the disk, respectively, and

$$S = \frac{2}{\sqrt{a^2 - b^2}} \tan^{-1}\left(\frac{\sqrt{a^2 - b^2}}{b}\right), \quad \text{for } b < a. \tag{A7}$$

Hence, the averaged friction coefficient for random-oriented sedimentation or creaming is [28]

$$f_{\text{eff}} = \frac{3}{\frac{1}{f_{\perp}} + \frac{2}{f_{\parallel}}} \tag{A8}$$

and

$$U_0 = \frac{2\Delta\rho\pi a^3 G}{f_{\text{eff}}\xi}, \tag{A9}$$

where G is the centrifugation acceleration.

[1] T. W. Oppel, W. K. Myers, and C. S. Keefer, J. Clin. Invest. **12**, 291 (1933).
[2] P. Y. Cheng and H. K. Schachman, J. Polym. Sci. **16**, 19 (1955).
[3] D. Lakehal, Int. J. Multiph. Flow **28**, 823 (2002).
[4] K. E. Davis, W. B. Russel, and W. J. Glantschnig, J. Chem. Soc., Faraday Trans. **87**, 411 (1991).
[5] P. N. Segre, E. Herbolzheimer, and P. M. Chaikin, Phys. Rev. Lett. **79**, 2574 (1997).
[6] W. Lee, A. Chan, M. A. Bevan, J. A. Lewis, and P. V. Braun, Langmuir **20**, 5262 (2004).
[7] G. G. Stokes, Trans. Cambridge Philos. Soc. **9**, 8 (1851).
[8] J. Perrin, J. Phys. Theor. Appl. **9**, 5 (1910).
[9] S. C. Glotzer and M. Solomon, Nature Mater. **6**, 557 (2007).
[10] F. N. Weber, R. L. Steere, H. G. Kim, D. W. Kupke, R. D. Rose, and R. M. Elton, Science **140**, 1090 (1963).
[11] Z. Dogic, A. P. Philipse, S. Fraden, and J. K. G. Dhont, J. Chem. Phys. **113**, 8368 (2000).
[12] M. B. Mackaplow and E. Shaqfeh, J. Fluid Mech. **376**, 149 (1998).
[13] D. Saintillan, E. Darve, and E. Shaqfeh, J. Fluid Mech. **563**, 223 (2006).
[14] B. Metzger, J. E. Butlerz, and E. Guazzelli, J. Fluid Mech. **575**, 307 (2007).
[15] R. H. Davis, Phys. Fluids A **3**, 2051 (1991).
[16] A. Holzer and M. Sommerfeld, Powder Technol. **184**, 361 (2008).
[17] V. M. Salokhe and N. B. Quang, J. Terramech. **32**, 231 (1995).
[18] M. Gray, Z. Xu, and J. Masliyah, Phys. Today **62**(3), 31 (2009).
[19] O. W. Moe, Lancet **367**, 333 (2006).
[20] S. M. Jogun and C. F. Zukoski, J. Rheol. **43**, 847 (1999).
[21] G. K. Batchelor, J. Fluid Mech. **52**, 245 (1972).
[22] S. E. Paulin and B. J. Ackerson, Phys. Rev. Lett. **64**, 2663 (1990).
[23] J. F. Richardson and W. N. Zaki, Chem. Eng. Sci. **3**, 65 (1954).
[24] R. Buscall, J. W. Goodwin, R. H. Ottewill, and T. F. Tadros, J. Colloid Interface Sci. **85**, 78 (1982).
[25] G. K. Batchelor and C. S. Wen, J. Fluid Mech. **124**, 495 (1982).
[26] F. Capuani, I. Pagonabarraga, and D. Frenkel, J. Chem. Phys. **124**, 124903 (2006).
[27] F. M. van der Kooij, K. Kassapidou, and H. N. W. Lekkerkerker, Nature (London) **406**, 868 (2000).
[28] F. M. van der Kooij, A. P. Philipse, and J. K. G. Dhont, Langmuir **16**, 5317 (2000).
[29] D. Frömer and D. Lerche, Arch. Appl. Mech. **72**, 85 (2002).
[30] T. Sobisch and D. Lerche, Colloid Polym. Sci. **278**, 369 (2000).
[31] Z. Cheng, P. M. Chaikin, and T. G. Mason, Phys. Rev. Lett. **89**, 108303 (2002).
[32] L. Y. Sun, W. J. Boo, D. H. Sun, A. Clearfield, and H. J. Sue, Chem. Mater. **19**, 1749 (2007).
[33] D. Sun, H.-J. Sue, Z. Cheng, Y. Martinez-Raton, and E. Velasco, Phys. Rev. E **80**, 041704 (2009).
[34] A. F. Mejia, P. He, D. Luo, M. Marquez, and Z. Cheng, J. Colloid Interface Sci. **334**, 22 (2009).
[35] D. Lerche, J. Dispersion Sci. Technol. **23**, 699 (2002).
[36] H. Shimizu, J. Chem. Phys. **37**, 765 (1962).
[37] W. R. Whalley and C. E. Mullins, Eur. J. Soil Sci. **43**, 531 (1992).
[38] J. K. G. Dhont, *An Introduction to Dynamics of Colloids*, 2nd ed. (Elsevier, New York, 1996).
[39] D. Costa, J. Hansen, and L. HarNau, Mol. Phys. **103**, 1917 (2005).
[40] J. Happel and H. Brenner, *Low Reynolds Number Hydrodynamics* (Prentice-Hall, Englewood Cliffs, NJ, 1965).
[41] B. J. Berne and R. Pecora, *Dynamic Light Scattering: With Applications to Chemistry, Biology, and Physics* (Dover, Mineola, NY, 2000).
[42] *Handbook of Data on Organic Compounds*, 3rd ed., edited by D. R. Lide and G. W. A. Milne (CRC, Cleveland, 1994).